

# POLYGONAL KNOT SPACE NEAR ROPELENGTH-MINIMIZED KNOTS

KENNETH C. MILLETT, MICHAEL PIATEK, AND ERIC RAWDON

ABSTRACT. For a polygonal knot  $K$ , it is shown that a tube of radius  $R(K)$ , the polygonal thickness radius, is an embedded torus. Given a thick configuration  $K$ , perturbations of size  $r < R(K)$  define satellite structures, or local knotting. We explore knotting within these tubes both theoretically and numerically. We provide bounds on perturbation radii for which we can see small trefoil and figure-eight summands and use Monte Carlo simulations to approximate the relative probabilities of these structures as a function of the number of edges.

## 1. INTRODUCTION

Equilateral polygonal knots have been used widely as statistical models of macromolecules such as DNA. For a fixed number of edges  $n$  these knots inhabit a space  $Equ(n)$  whose structure reflects the possibility of changes in conformation subject to constraints such as the preservation of edge lengths and the prohibition of singularities such as one edge passing through another. This space is a subspace of the space of polygonal knots  $Geo(n)$  in which the edges may change in length but not in number and again, edges may not pass through each other. In this paper, we will study the behavior of equilateral knots under spatial perturbation of their vertices in  $Geo(n)$ . These perturbations may be thought of as changes in the configuration during which we suspend the constraint of edge length preservation and, when the scale of perturbation is sufficiently large, the prohibition against edges passing through other edges. We will require that the number of edges remains the same. Of special interest are the “thick” equilateral knots, representatives of the knot type in which the edges are quite separated. We explore the structure of local knotting near these “thick” knots which, by our definition, will be those which occur from perturbations within a thick tube surrounding the knot. Global knotting changes can occur when the size of the perturbation exceeds the radius of this tube.

Key to this study is the “Tube Theorem” (Theorem 7.1 in Section 7) describing the explicit structure of a uniformly large embedded solid

torus containing the knot as its center. The radius of this tube about the knot is the thickness radius of the knot conformation  $R(K)$  defined in [22, 23]. The theorem and the associated value of  $R(K)$  are the starting point of our analysis. The precise definition of  $R(K)$  and a discussion of some of its properties are contained in the next section.

Perturbations of the knot that remain within this tube define satellites of the knot. The nature of these perturbations vary from being equivalent polygonal knots, for very small perturbations, to those which are connected sums with small trefoils (a “local knot”) and, finally, to those satellites that may constitute a more complex structure distributed across the entire tube but whose structure still derives from a local perturbation of the core knot. Once the scale of the perturbation allows the edges to pass beyond the boundary of the tube, crossings between arclength-distant edges in the knot may occur and a “global” change in knotting is possible, but for the purpose of this note, we concentrate on the perturbations causing local knotting changes.

From the perspective of  $Equ(n)$ , as a subspace of  $Geo(n)$ , the perturbed knots can be understood as nearby neighbors of the knot  $K$  in knot space and can be expected to have structure that bears a close resemblance to that of  $K$ . We will see that the critical perturbation parameters that quantify the extent of structural change are the thickness radius of the knot and the number and length of its edges. So long as the scale of the perturbation is sufficiently small in terms of these quantities, the resulting knot will be geometrically equivalent, that is lying in the same connected component of  $Geo(n)$  as does the knot  $K$ . If the relationship between the number of edges, edge length, and the thickness radius allows, the neighbors may contain small trefoil summands or summands of other small knots. This relationship forms the basis of the passage from a “rigid” knot regime to one whose behavior more closely resembles that of smooth knots in a thickest state. That is to say, for some equilateral knots, it is impossible to form local knots even in its thickest conformation due to the small number of edges. The minimal number of edges required to form a local knot under perturbation in an equilateral knot type is one possible indicator of the passage from being a “rigid” knot to a structure that permits sufficient flexibility of motion to better model the behavior of large knots.

For sufficiently large knots, as expressed in terms of the relationship between the number of edges and the knot’s thickness radius, it is possible to encounter perturbations that are organized across its entire length so as to produce more complex satellite structures. Such perturbations require more edges than are necessary to produce local knotting and provide a second point at which the character of the knot

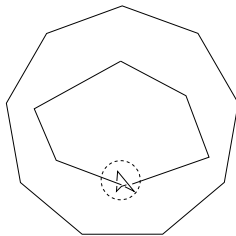


FIGURE 1. A nine edge trefoil satellite of the trivial knot.

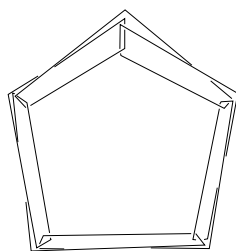


FIGURE 2. A complex 25 edge satellite of the trivial knot.

may be thought of as changing. For example, for the unknot, nine edges are required in order that a (rather large) perturbation within the tube gives rise to a local trefoil as shown in Figure 1. By way of contrast, a rough analysis estimates that at least 25 edges are required for a satellite that is not a sum of local knots as shown in Figure 2. So long as the relationship between the thickness radius and the edge lengths permit, we will see that the perturbations of edges can remain within the tube and exhibit increasingly complex local knotting structure and an exponential growth in occurrence and complexity as expected. This structure is characteristic of the neighborhood, as measured by the perturbation scale, of the  $K$  in knot space.

In this paper we will provide both a theoretical analysis and Monte Carlo simulation data that illuminate the local structure of knot space as measured by the perturbation scale associated to an equilateral knot. The theoretical dimension will provide estimates of the scale of perturbation required to attain different satellite structures while the Monte Carlo data will relate these estimates to observation. Using a random sampling of the set of perturbations and a HOMFLY polynomial analysis of this data, we are able to study and characterize the complexity of knots nearby the knot determining core of the tube. One may think of this effort as an indirect strategy to study the local geometry and topology of knot space. For example, we analyze the number of edges

required to obtain different satellite structures (usually occurring as connected sums of prime knots) as well as the growth in the relative frequency as a function of the number of edges. These are exhibited in the differences in the data at the local scale near the thickest trivial, trefoil, and figure-eight knots.

## 2. BACKGROUND ON ROPELENGTH

We explore perturbations about ropelength-minimized equilateral polygonal knots, the so-called *ideal knots*. For completeness, we will include background on ropelength for smooth knots, which for the sake of this discussion means  $C^2$ , and for polygonal knots, in which edge lengths are no longer required to be equal.

The ropelength of a knot was defined in [1] and the basic theory developed in [14], although similar ideas appeared previously [10, 13, 19]. Smooth ropelength models an idealize rope as a non self-intersecting tube with a knot as the filament-like core.

**Definition 2.1.** For a  $C^2$  smooth knot  $K$  and  $x \in K$ , let  $D_r(x)$  be the disk of radius  $r$  centered at  $x$  lying in the plane normal to the tangent vector at  $x$ . Let

$$R(K) = \sup\{r > 0 : D_r(x) \cap D_r(y) = \emptyset \text{ for all } x \neq y \in K\}.$$

The quantity  $R(K)$  is called the *thickness radius* of  $K$ . Define the *ropelength* of  $K$  to be

$$\text{Rope}(K) = \text{Length}(K)/R(K)$$

where  $\text{Length}(K)$  is the arclength of  $K$ .

For a fixed knot configuration,  $R(K)$  is the radius of a thickest tube that can be placed about  $K$  without self-intersection. Given a knot surrounded by an impenetrable tube of some radius, there are two types of interactions between normal disks that restrict the conformations that can be obtained. First, the tube cannot bend too quickly, a restriction on the curving of the core. Second, two arclength-distant points in the core cannot be any closer than twice the radius of the tube, a restriction on the distance between pairs of points bounded away from the diagonal of  $K \times K$ . These intuitive observations are captured by the quantities below and the subsequent lemma.

**Definition 2.2.** For a  $C^2$  knot  $K$  with unit tangent map  $T$ , let  $\text{MinRad}(K)$  be the minimum radius of curvature. The *doubly-critical self-distance* is the minimum distance between pairs of distinct points on the knot

whose chord is perpendicular to the tangent vectors at both of the points. In other words, let

$$DC(K) = \{(x, y) \in K \times K : T(x) \perp \overline{xy} \perp T(y), x \neq y\}$$

where  $\overline{xy}$  is the chord connecting  $x$  and  $y$ . Define the *doubly-critical self-distance* by

$$dcsd(K) = \min\{\|x - y\| : (x, y) \in DC(K)\},$$

where  $\|\cdot\|$  is the standard  $\mathbb{R}^3$  norm.

There is a fundamental relationship between  $R(K)$ ,  $MinRad(K)$ , and  $dcsd(K)$ .

**Lemma 2.3.** *Suppose  $K$  is a  $C^2$  knot. Then*

$$R(K) = \min\{MinRad(K), dcsd(K)/2\}.$$

*Proof.* See [14]. □

A surprising result from [14] establishes that, in fact, the doubly-critical self-distance can be replaced by the singly-critical self-distance, an idea attributed to J. O’Hara and N. Kuiper [20]. We prove a similar result for polygons in the next section.

**Proposition 2.4.** *Let*

$$SC(K) = \{(x, y) \in K \times K : T(x) \perp \overline{xy}, x \neq y\}$$

*and the singly-critical self-distance be  $scsd(K) = \min_{(x,y) \in SC(K)} \|x - y\|$ . Then*

$$R(K) = \min\{MinRad(K), scsd(K)/2\}.$$

*Proof.* See [14]. □

The thickness radius and ropelength definitions can be extended to  $C^{1,1}$  curves (see [12, 4, 7]). Since  $R(K)$  changes with scale and we are mainly interested in the “shape” of the optima, the scale-invariant ropelength is the quantity typically studied.

In [22, 23], the polygonal thickness radius and polygonal ropelength functions were defined in the spirit of the characterization in Lemma 2.3. Before we define this, we introduce some notation.

For an  $n$ -edge polygonal knot  $K$ , define the following:

- Let  $v_1, \dots, v_n$  be the vertices of  $K$ . For convenience, we implicitly take all subscripts modulo  $n$ .

- Let  $e_1, \dots, e_n$  be the edges of  $K$ , where  $e_i$  is the edge connecting  $v_i$  to  $v_{i+1}$ .
- Let  $|e_i|$  be the length of the edge  $e_i$ .
- Let  $angle(v_i)$  be the measure of the turning angle at  $v_i$  (see Figure 3).
- Given a knot  $K$  and  $x \in K$ , let  $d_x : K \rightarrow \mathbb{R}$  be defined by  $d_x(y) = \|x - y\|$ .

**Definition 2.5.** For a vertex  $v_i$  on an  $n$ -edge polygonal knot  $K$ , let

$$Rad(v_i) = \frac{\min\{|e_{i-1}|, |e_i|\}}{2 \tan(angle(v_i)/2)}$$

and

$$MinRad(K) = \min_{i=1, \dots, n} Rad(v_i).$$

Note that  $Rad(v_i)$  is the radius of a circular arc that can be inscribed at  $v_i$  so that the arc is tangent to both edges adjacent to  $v_i$  and the arc intersects the shorter adjacent edge at its midpoint (see Figure 3). We call  $y$  a *turning point* for  $x$  if  $d_x$  changes from increasing to decreasing or from decreasing to increasing at  $y$ . Let

$$DC(K) = \{(x, y) \in K \times K : x \neq y \text{ turning points of } d_y \text{ and } d_x \text{ respectively}\}.$$

Define the *doubly-critical self-distance* of  $K$  to be

$$dcsd(K) = \min\{\|x - y\| : (x, y) \in DC(K)\}.$$

We call a pair  $(x, y) \in DC(K)$  a *doubly critical pair*.

**Definition 2.6.** For a polygonal knot  $K$ , let

$$R(K) = \min\{MinRad(K), dcsd(K)/2\} \text{ (polygonal thickness radius)}$$

and

$$Rope(K) = \frac{Length(K)}{R(K)} \text{ (polygonal ropelength)}.$$

In [22, 23], it was shown that, under mild geometric hypotheses, for finer and finer inscribed polygonal approximations of a smooth knot  $K$ , the thickness radius and ropelength of the polygons converge to the respective values of  $K$ . In [24], we showed that the ropelength of polygonal optima converge to the minimum smooth ropelength and that a subsequence of the minimizing polygons converges pointwise to a smooth ropelength minimum.

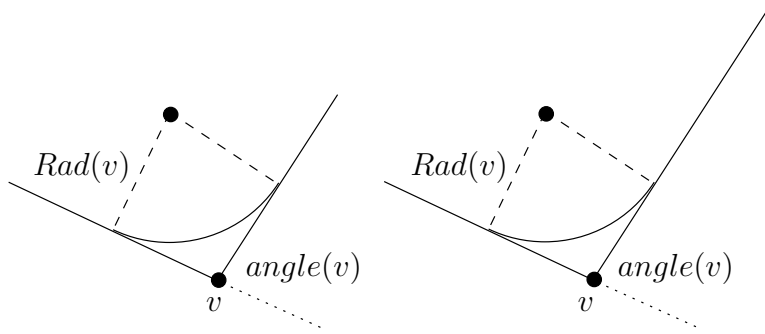


FIGURE 3. An arc of a circle of radius  $Rad(v)$  can be inscribed so that the arc is tangent at the midpoint of the shorter adjacent edge. On the left, the two adjacent edges have identical length, so the arc intersects both edges tangentially at the midpoints. On the right, the arc intersects the longer edge at a point short of the midpoint.

### 3. SELF-DISTANCE AND LEMMAS ABOUT POLYGONAL ARCS

In this section, we prove that polygonal thickness radius can be reformulated in terms of the singly-critical self-distance. This is the polygonal version of Proposition 2.4 and further shows how closely the polygonal thickness radius models the behavior in the smooth case. We need some definitions and lemmas before we can prove this result.

**Definition 3.1.** For a polygonal knot  $K$ , let  $MD(K)$  be the minimum distance between non-adjacent edges of  $K$  and  $MD(e, v)$  be the minimum distance between edge  $e$  and vertex  $v$ .

Notice that  $MD(K)$  is bounded above by the minimum edge length of  $K$ , which we denote  $MinEdge(K)$ .

**Definition 3.2.** For a polygonal knot  $K$ , let  $SC(K)$  consist of all pairs  $(x, y) \in K \times K$  such that  $x$  and  $y$  are on non-adjacent edges and  $y$  is a turning point which is a local minimum of  $d_x$ . Define the *singly-critical self-distance* of  $K$  by

$$scsd(K) = \min_{(x,y) \in SC(K)} \|x - y\|.$$

Since  $SC(K)$  is a closed set,  $scsd(K)$  is well-defined. We need the following three lemmas to recharacterize the polygonal thickness radius with  $scsd$  used in place of  $dcsd$ . The first provides a lower bound on the distance between an edge and the vertices of the adjacent edges.

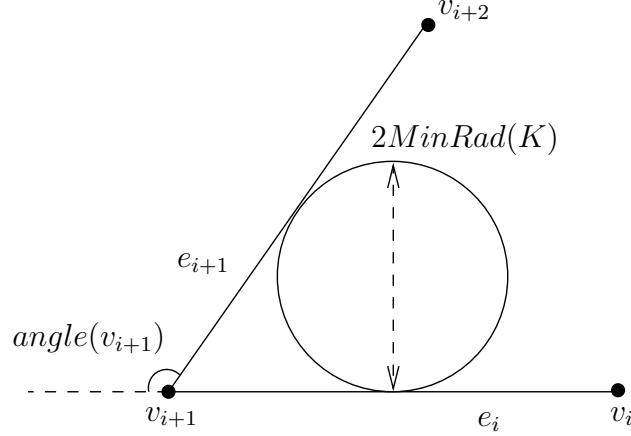


FIGURE 4. When  $\text{angle}(v_{i+1}) \geq \pi/2$ , the minimum distance from  $v_{i+2}$  to  $e_i$  is  $\geq 2 \text{MinRad}(K)$ .

**Lemma 3.3.** *For a polygonal knot  $K$ ,*

$$MD(e_i, v_{i+2}) \geq \min\{2 \text{MinRad}(K), \text{MinEdge}(K)\}.$$

*In particular, when  $\text{angle}(v_{i+1}) \geq \pi/2$ , we have*

$$MD(e_i, v_{i+2}) \geq 2 \text{MinRad}(K).$$

*A similar result holds for  $MD(e_i, v_{i-1})$ .*

*Proof.* If  $\text{angle}(v_{i+1}) \leq \pi/2$ , then the minimum distance is realized at  $v_i$  and  $v_{i+1}$  which is at least  $\text{MinEdge}(K)$ . If  $\text{angle}(v_{i+1}) > \pi/2$ , then  $2 \text{MinRad}(K) \leq \frac{|e_i|}{\tan(\text{angle}(v_{i+1})/2)}$  and  $d(v_i, e_{i+1}) = |e_i| \sin(\pi - \text{angle}(v_{i+1}))$  (see Figure 4). Simple trigonometry show that  $2 \text{MinRad}(K) \leq d(v_i, e_{i+1})$ .  $\square$

The *total curvature* between two points  $tc(x, y)$  on a polygon is the minimum (over the two arcs connecting  $x$  to  $y$ ) of the sum of the turning angles along the arc, including the angle at  $x$  and/or  $y$  if one or both happen to be vertices. The total curvature is used to recharacterize polygonal  $R(K)$  in Lemma 3.5.

**Lemma 3.4.** *Suppose  $x, y$  are points on a polygonal knot  $K$  and let  $TC(K) = \{(x, y) \in K \times K : tc(x, y) \geq \pi\}$ .*

- (a) *If  $tc(x, y) < \pi$ , then  $(x, y)$  is not a doubly critical pair.*
- (b) *If  $tc(x, y) \geq \pi$ , then  $\|x - y\| \geq 2 R(K)$ .*
- (c) *If  $(x, y) \in TC(K)$  is on the boundary of  $TC(K)$ , then  $\|x - y\| \geq 2 \text{MinRad}(K)$ .*

*Proof.* See [23].  $\square$



The following is a characterization of polygonal  $R(K)$  that will be used in the proof of Theorem 3.6, the polygonal version of Proposition 2.4.

**Lemma 3.5.** *For a polygonal knot  $K$ ,*

$$R(K) = \min \left\{ \text{MinRad}(K), \min_{(x,y) \in TC(K)} \|x - y\|/2 \right\}.$$

*Proof.* See [23]. □

**Theorem 3.6.** *For a polygonal knot  $K$ ,*

$$R(K) = \min \{ \text{MinRad}(K), \text{scsd}(K)/2 \}.$$

*Proof.* Usually, we will have  $\text{scsd}(K) \leq \text{dcsd}(K)$ . However, recall that  $\text{scsd}(K)$  is defined only over pairs  $(x, y)$  where  $y$  is a local minimum turning point of  $d_x$  while  $\text{dcsd}(K)$  is defined over all doubly turning pairs, in particular those which are local maxima.

Suppose  $\text{scsd}(K) > \text{dcsd}(K)$ . We show that in such a case  $R(K) = \text{MinRad}(K) \leq \text{dcsd}(K)/2 < \text{scsd}(K)/2$ . Suppose  $\text{dcsd}(K)$  is realized at the pair  $(x_0, y_0) \in DC(K)$ . If  $x_0$  is a local minimum for  $d_{y_0}$  or  $y_0$  is a local minimum for  $d_{x_0}$ , then  $\text{scsd}(K) \leq \text{dcsd}(K)$ . Thus,  $x_0$  and  $y_0$  are local maxima for  $d_{y_0}$  and  $d_{x_0}$  respectively. Note that  $\min_{(x,y) \in TC(K)} \|x - y\| \leq \text{dcsd}(K)$  by Lemma 3.4(a). If  $\text{dcsd}(K)/2 < \text{MinRad}(K)$  then Lemma 3.5 tells us that  $\min_{(x,y) \in TC(K)} \|x - y\| = \text{dcsd}(K)$ . In other words,  $(x, y)$  must be a global minimum of the distance function over  $TC(K)$ . By Lemma 3.4(c), this global minimum cannot occur on the boundary of  $TC(K)$ , and, thus, the points  $x_0$  and  $y_0$  must be minima for  $d_{y_0}$  and  $d_{x_0}$  respectively. Thus,  $R(K) = \text{MinRad}(K)$  whenever  $\text{scsd}(K) > \text{dcsd}(K)$ , and the result holds.

So we can assume that  $\text{scsd}(K) \leq \text{dcsd}(K)$ . Certainly, if  $\text{MinRad}(K) \leq \text{scsd}(K)/2 \leq \text{dcsd}(K)/2$ , then the result holds. So what remains is to show that if  $\text{scsd}(K)/2 < \text{MinRad}(K)$ , then  $\text{scsd}(K) = \text{dcsd}(K)$ .

Suppose  $\text{scsd}(K)/2 < \text{MinRad}(K)$  and  $(x, y)$  is a pair in  $SC(K)$  that realizes  $\text{scsd}(K)$ . In the following arguments, we assume that  $\text{scsd}(K) < \text{dcsd}(K)$  and obtain the contradiction that  $\text{scsd}(K) < \|x - y\|$ .

Consider  $B$ , the ball of radius  $\text{scsd}(K)$  centered at  $y$ . We consider the cases where  $x$  and  $y$  are vertex or non-vertex points. When  $x$  is a non-vertex point (i.e. lies in the interior of an edge), let  $\alpha_x$  be the edge containing  $x$  and define  $\alpha_y$  analogously.

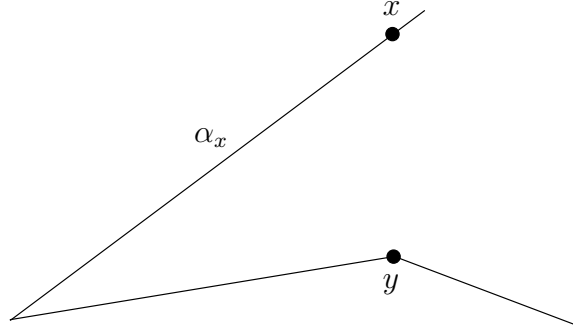


FIGURE 5. When  $y$  is a local minimum for  $d_x$  and  $\alpha_x$  is adjacent to one of the edges containing the vertex  $y$ , the turning angle between the edges must be at least  $\pi/2$ .

**Case 1:**  $y, x$  both non-vertex points

Since  $(x, y) \in SC(K)$ ,  $\alpha_x$  and  $\alpha_y$  are non-adjacent. Since  $(x, y)$  is not doubly critical,  $\alpha_x$  pierces  $B$  at  $x$ . Since  $y$  is interior to  $\alpha_y$ ,  $y$  divides  $\alpha_y$  into two pieces, say  $\alpha_y^1$  and  $\alpha_y^2$ . Since  $(x, y) \in SC(K)$ ,  $\overline{xy} \perp \alpha_y$  at  $y$ , so  $\|x - y\|$  is a local minimum of  $d_x$ . Thus, there exist  $y_1 \in \alpha_y^1$  and  $y_2 \in \alpha_y^2$ , both interior to  $\alpha_y$  such that

$$\|x - y_1\| > \|x - y\| \text{ and } \|x - y_2\| > \|x - y\|.$$

Furthermore, there exists an  $x'$  arbitrarily close to  $x$  on  $\alpha_x \cap B$  such that

$$\|x' - y\| < \|x - y\|, \|x' - y_1\| > \|x - y\|, \text{ and } \|x' - y_2\| > \|x - y\|.$$

Thus, there exists a point  $y'$  between  $y_1$  and  $y_2$  (interior to  $\alpha_y$ ) that minimizes the distance to  $x'$ . Then  $(x', y') \in SC(K)$  with  $\|x' - y'\| < \|x - y\| = scsd(K)$ , which is a contradiction.

**Case 2:**  $y$  is a vertex and  $x$  is non-vertex

Then  $\alpha_x$  pierces  $B$  and  $y$  is a local minimum of  $d_x$ . The argument from Case 1 holds unless  $y$  is a vertex on an edge adjacent to  $\alpha_x$ . In such a case, we have the situation in Figure 5. The turning angle from adjacent edge containing  $y$  to  $\alpha_x$  must be at least  $\pi/2$ . The result follows by Lemma 3.3.

**Case 3:**  $y$  is non-vertex,  $x$  is a vertex

Let  $\alpha_x^1$  and  $\alpha_x^2$  be the edges adjacent to  $x$ . Note that exactly one of the adjacent edges  $\alpha_x^1$  and  $\alpha_x^2$  must pierce  $B$  or else  $(x, y)$  is doubly critical. Without loss of generality, assume that  $\alpha_x^1$  pierces  $B$ . Two things can happen. If  $\alpha_x^1$  is adjacent to  $\alpha_y$ , then (as in Case 2) the turning angle must be  $\pi/2$  and Lemma 3.3 gives us the result. Otherwise, the argument from Case 1 holds.

**Case 4:**  $y, x$  are both vertices

Then  $\alpha_x$  pierces  $B$  and  $y$  is a local minimum for  $d_x$ . The argument from Case 1 holds unless an edge containing  $x$  and an edge containing  $y$  are adjacent, in which case the vertex between the two edges must have a turning angle of at least  $\pi/2$  and Lemma 3.3 gives us the desired result.  $\square$

The previous theorem says that if  $dcsd(K) < MinRad(K)$ , then  $scsd(K) = dcsd(K)$ . The following corollary follows immediately.

**Corollary 3.7.** *For a polygonal knot  $K$ ,*

$$MD(K) \geq \min\{2R(K), MinEdge(K)\}.$$

The following is a corollary to Lemma 3.5 and shows that we need only consider pairs from  $DC(K)$  that are minima for the distance function in order to characterize  $R(K)$  for polygons. Note however, that  $mdcsd(K)$  can be empty in which case we set  $mdcsd(K) = \infty$ , e.g. on a regular  $n$ -gon where  $n$  is odd.

**Proposition 3.8.** *Let*

$$MDC(K) = \{(x, y) \in K \times K : x \neq y \text{ turning point minima of } d_y \text{ and } d_x \text{ respectively}\}.$$

and

$$mdcsd(K) = \min\{\|x - y\| : (x, y) \in MDC(K)\}.$$

Then

$$R(K) = \min\{MinRad(K), mdcsd(K)/2\}.$$

*Proof.* Note that  $dcsd(K) \leq mdcsd(K)$ . If  $MinRad(K) \leq dcsd(K)/2$ , then the result holds.

If  $dcsd(K)/2 < MinRad(K)$ , then  $\min_{(x,y) \in TC(K)} \|x - y\| = dcsd(K)$ . Thus, we know that  $dcsd(K)$  is realized at a pair  $(x, y)$  where  $y$  and  $x$  are minima of  $d_x$  and  $d_y$  respectively, as desired.  $\square$

Now we have established some properties of the polygonal thickness radius. Next we complete a Monte Carlo simulation to understand the structure of the thick tube about a knot.

#### 4. LOCAL STRUCTURE OF EQUILATERAL KNOT SPACE

A polygonal knot  $K$  is determined by a sequence of  $n$  points in three-space, the vertices of  $K$ . These vertices determine a sequence of edges (straight line segments) connecting the vertices, including an edge from the last to the first of the vertices. It is required that the vertices are distinct and that the edges meet only at the common vertex with the adjacent edge sharing the vertex. In fact, this approach provides each

knot with a first vertex and an orientation, since the sequence determines a specific second vertex and therefore a direction along the knot. These knots, then, are described by a single point in the Euclidean space of dimension  $3n$  and the entire collection of such knots determines an open subset  $Geo(n)$  of this Euclidean space. The collection of knots whose edge lengths are all equal determines the subset of equilateral knots  $Equ(n)$  of  $Geo(n)$ . Let  $Edge(K)$  denote the length of the edges of a knot  $K \in Equ(n)$ . If  $K$  and  $K'$  are two knots in  $Geo(n)$ , we define the distance between  $K$  and  $K'$  to be equal to the largest standard Euclidean distance between the corresponding vertices of  $K$  and  $K'$ . Using this definition of distance between knots in  $Geo(n)$ , we describe the neighborhood  $N(K, r)$  of  $K$  in  $Geo(n)$  to be those knots in  $Geo(n)$  within distance  $r$  of  $K$ . With this definition in mind, we observe that any perturbation of the vertices of an equilateral knot  $K$  of scale no larger than  $r$  specifies a knot in the neighborhood  $N(K, r)$ . As a consequence, the analysis of the possible knots occurring with perturbation scale less than or equal to  $r$  provides a description of the knots occurring in  $N(K, r)$ .

We will need Schur's Theorem [5] for our subsequent analysis of the necessary perturbation size required to form different types of local knotting.

**Lemma 4.1.** *Let  $C$  and  $C^*$  be two piecewise linear curves of the same length, such that  $C$  forms a simple convex plane curve with the chord connecting its endpoints. Let  $s$  be the arclength parameter for  $C$  and  $C^*$ . When  $s$  corresponds to a vertex of  $C$  (and  $C^*$ ), let  $angle(s)$  be the turning angle at a vertex, and  $angle^*(s)$  be the corresponding angle on  $C^*$ . Let  $d$  and  $d^*$  be the distances between the endpoints of  $C$  and  $C^*$ , respectively. Then, if  $angle^*(s) \leq angle(s)$ , we have  $d^* \geq d$ .*

Thus, given an equilateral polygon with a fixed edge length and maximum turning angle  $\theta_{max}$ , we can find a lower bound for the distance between vertices by analyzing a planar polygon with the same edge lengths and a constant turning angle of  $\theta_{max}$ .

We now analyze the size of perturbation required to create local knotting. Note that the size of perturbation will depend on how much the polygon is curving, namely in that more curving implies that vertices can be closer together (see Figure 6).

**Theorem 4.2.** *If  $K$  is a knot in  $Equ(n)$  and the scale of perturbation  $r$  is smaller than*

$$\min \left\{ \frac{1}{2} Edge(K) \frac{12R(K)^2 - Edge(K)^2}{4R(K)^2 + Edge(K)^2}, R(K) \right\},$$



FIGURE 6. The perturbation size required to collect four vertices in a small ball changes depending on the curvature of the polygon, detected here by the *MinRad* term of  $R(K)$ .

then all knots in  $N(K, r)$  are equivalent to  $K$  in  $Geo(n)$ .

*Proof.* In Section 7, we prove the Tube Theorem (Theorem 7.1). For the sake of this proof, the Tube Theorem says that any knot change must occur within the tube of radius  $R(K)$  about the knot, what we term local knotting. Thus, any change in knot type must occur on an arc of  $K$  whose total curvature is  $< \pi$  by Lemma 3.4(b).

A local trefoil knot can occur at any radius beyond the value at which four points can coalesce at a single point. A planar gon whose radius of curvature is equal to  $R(K)$  and edge length is  $Edge(K)$  has four consecutive vertices meeting at a common point at a minimum distance of  $R_0 = \frac{1}{2}Edge(K) \frac{12R(K)^2 - Edge(K)^2}{4R(K)^2 + Edge(K)^2}$ . Applying Schur's Theorem, we get that the distance between the endpoints of a four-vertex arc is at least this value.  $\square$

For an equilateral unknot with  $n$  edges inscribed in a circle of radius one, the edge length is  $2 \sin(\pi/n)$  and the thickness radius is  $\cos(\pi/n)$ . An analysis shows that for less than nine edges, no local knotting is possible, i.e. the size of the tube is smaller than the minimum perturbation size needed to bring four consecutive vertices to a common point. It might be easier to think of the thickness radius relative to the size of an edge length here. We include both the raw measurement of thickness radius and the thickness radius in relation to the size of an edge. For nine edges, this term, 0.8660 (or 1.2660 *Edge*), is smaller than the thickness radius, 0.9396 (or 1.3737 *Edge*), implying the possibility of local knotting, i.e. knotting occurring within the tubular neighborhood of the knot with radius equal to the thickness radius as shown in Figure 1. In this range, only trefoil knots can arise. This analysis is specific to the standard regular  $n$ -gon, giving the minimum perturbation required to bring together the required four vertices as  $\sin(3\pi/n)$  in order to create a local trefoil. Applying the same method of analysis to the creation of a local figure-eight knot where five consecutive vertices must come together, the minimum perturbation is  $\sin(4\pi/n)$ . This shows that at least 11 edges are required. In this case the minimum perturbation is 1.6144 *Edge* compared to a thickness radius of 1.7028 *Edge*.

In each of these limiting cases we should expect the proportion of the neighborhood of the unknot consisting of trefoils and figure-eight knots to be very very small.

To explore these and other features of the local structure, we have undertaken a Monte Carlo sampling of the nearby knots through a random perturbation of the vertices. While a fuller discussion of the data occurs later in this note, it may be helpful to introduce some aspects of the data presently so as to give a more accurate sense of the local structure of equilateral knot space. For  $n = 9$ , one can make a rough calculation that will give an estimate of the probability of occurrences of trefoil summands in the perturbation. One first calculates the probability that four consecutive vertices coalesce in a small ball and then multiplies this by the probability of a trefoil in  $Geo(6)$  [16]. This crude estimate of the probability of a trefoil summand is thereby calculated to be  $3.1974 \times 10^{-16}$  or, about 3 chances in  $10^{16}$  cases. As a consequence, it is not surprising that we have not encountered trefoils in testing five million cases with nine edges. For  $n = 10$ , the probability is  $8.1194 \times 10^{-13}$  relatively speaking, rather more likely, about 8 chances in  $10^{13}$  cases, but still too small to expect an observation in only five million cases. For  $n = 11$ , when we first have the possibility of figure-eight knots as well as trefoils, the theoretical lower-bound estimate of the probability of trefoil knots increases to  $6.0951 \times 10^{-11}$  and, for  $n = 12$ , to  $1.0837 \times 10^{-9}$ . The first actual observation of a trefoil knot in our study occurred at  $n = 11$  in a sample of  $5 \times 10^6$  cases. This data provides a Monte Carlo estimate of the probability of a trefoil knot at  $n = 11$  within the tube of maximal thickness radius of  $1.2 \times 10^{-6}$ , rather larger than the theoretical lower bound estimate. The first observed figure-eight knot, in  $5 \times 10^6$  trials, occurred for  $n = 16$ .

Once local knotting becomes possible, we can ask “For a fixed number of edges, how large of a perturbation is necessary in order that a local trefoil might be observed?” We did a specific analysis for the case of regular 32-gons. The regular 32-gon inscribed in the circle of radius one has a minimum perturbation of 0.2903 theoretically required for one or more trefoil summands, 0.3827 for connected sums of local trefoils and local figure-eight knots, and 0.4714 for more complicated summands or other satellite knots. The thickness radius of the regular 32-gon is 0.9952, approximately one, so that a wide range of satellite knotting should be anticipated from perturbations constrained to lie within the tube. A Monte Carlo exploration of the perturbations of increasing scale, with a sample size of  $2 \times 10^7$ , is consistent with these predictions. The first trefoils occur when the maximum perturbation radius is 0.3981 and figure-eight knots and connected sums of trefoils

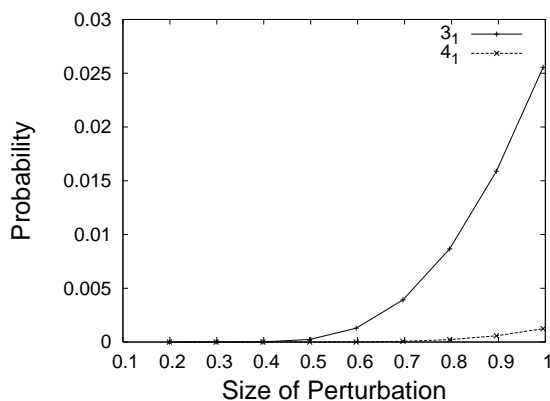


FIGURE 7. The proportion of perturbed 32-gons containing exactly one trefoil or figure-eight knot as a function of the size of the perturbation.

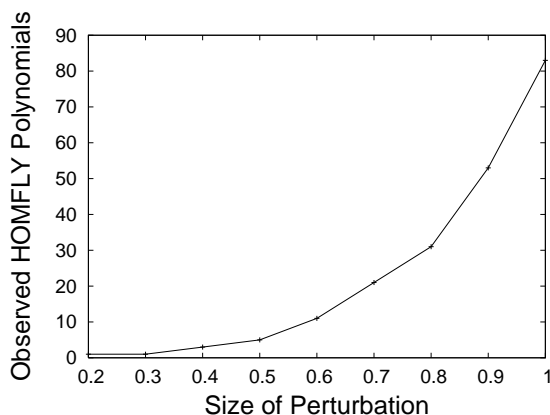


FIGURE 8. The number of distinct HOMFLY polynomials of knots arising from perturbations of the vertices of the regular 32-gon as a function of the size of the perturbation in a sample of size  $2 \times 10^7$ .

occur when the maximum perturbation radius is 0.4976 (see Figure 7). The complexity in the knotting increases rapidly with increasing perturbation size within the tube as is shown in the graph in Figure 8. Within the range of perturbations remaining inside the tube, connected sums of up to three trefoils as well as other more complex knots are observed.

**Theorem 4.3.** *If the scale of perturbation  $r$  is larger than*

$$\frac{1}{2} \text{Edge}(K) \frac{12 R(K)^2 - \text{Edge}(K)^2}{4R(K)^2 + \text{Edge}(K)^2}$$

but less than

$$\min \left\{ 4 \operatorname{Edge}(K) R(K) \frac{4R(K)^2 - \operatorname{Edge}(K)^2}{(4R(K)^2 + \operatorname{Edge}(K)^2)^{\frac{3}{2}}}, R(K) \right\},$$

then connected sums of local trefoils may occur, but nothing more complex is possible.

*Proof.* Analogously, as in the previous theorem, we calculate the smallest perturbation that allows five vertices to coalesce in a small ball, necessary for the occurrence of a figure-eight knot. The fact that nothing more complex is possible is a consequence of the fact that the perturbation limit does not allow any of the vertices adjacent to those determining a local trefoil to meet a surrounding small ball containing the local trefoil. Thus, a connected sum with small trefoils is all that can occur.  $\square$

**Theorem 4.4.** *If the scale of perturbation  $r$  is larger than*

$$4 \operatorname{Edge}(K) R(K) \frac{4R(K)^2 - \operatorname{Edge}(K)^2}{(4R(K)^2 + \operatorname{Edge}(K)^2)^{\frac{3}{2}}}$$

but less than

$$\min \left\{ \frac{1}{2} \operatorname{Edge}(K) \frac{80R(K)^4 - 40R(K)^2 \operatorname{Edge}(K)^2 + \operatorname{Edge}(K)^4}{(4R(K)^2 + \operatorname{Edge}(K)^2)^2}, R(K) \right\},$$

then connected sum of local trefoils and figure-eight knots may occur, but nothing more complex is possible.

*Proof.* The proof of this theorem follows from the estimate of the minimal distance needed to bring six vertices into a small ball. It is at this point, where we must consider bringing six or more vertices together that more complex knots, those polygonal knots with edge number eight, are theoretically possible [2, 3].  $\square$

## 5. MONTE CARLO EXPLORATIONS OF THE LOCAL STRUCTURE OF EQUILATERAL KNOT SPACE

As with the global character of the entirety of the knot space  $\operatorname{Geo}(n)$ , the complexity of knotting for perturbations of a knot staying within its maximal tube increases exponentially as a function of the number of edges. In a first study, we illustrate the structure of local knotting by a numerical study of perturbations of the unknot.

We generated random knots within tubes about thick unknots, trefoils, and figure-eight knots with various numbers of edges. The host knot is a ropelength-minimized equilateral polygon computed by TOROS [21] using a simulated annealing algorithm. As such, these are not



absolute polygonal ropelength-minima, but are good approximations. Because of the difference in the complexities of the knots, it took many more edges to see compositions with trefoils within the trefoil tube than the unknot tube. Therefore, we used different numbers of edges for the different knots. For a given knot and number of edges, we generated  $5 \times 10^6$  random knots by perturbing each vertex by a random vector uniformly distributed in a ball of radius  $R(K)$ . The knot types were determined by computing the HOMFLY polynomial of the perturbed knot using the Millett-Ewing program [9]. Therefore, strictly speaking, we are computing the relative occurrence of the HOMFLY polynomial. However, for the range of this study, these provide an accurate representation of the population of knots and the local incidence of these knots parallels their occurrence in knot space.

At this point, the Millett-Ewing program can compute the HOMFLY polynomial for knots with at most 999 crossings. For the figure-eight knot with more than 500 edges, we obtained a significant number of knots with more than 1000 crossings. Therefore, we could not continue the graphs beyond 500 edges for the trefoil and figure-eight. However, the graphs suggest that the behavior of the relative probabilities is consistent and robust.

As is the case in studies of other knot spaces, such as  $Geo(n)$ ,  $Equ(n)$ , and the unit lattice  $\mathbb{Z}^3$ , the unknot is, for small numbers of edges, the most probable knot and the probability decays exponentially. We fit a curve to the probabilities using the fitting function

$$a(n - n_0)^b e^{-kn - ln^2}$$

where  $n$  denotes the number of edges and  $a$ ,  $b$ ,  $k$ ,  $l$ , and  $n_0$  are fitting parameters. We have tested the quality of fit provided by a range of functions employed in various studies, including this one, and find that this choice is appropriate for the goals of this project [18]. From the graphs, one can see that the functions fit the curves well.

The graphs of the proportion of unknots in the thick tube about the unknot, trefoil, and figure-eight are shown in Figs. 9, 11, and 13. The proportion of trefoil knots and figure-eight knots, shown in Figs. 10, 12, and 14, demonstrate the extent of similarity of the data regardless of the core knot. While there are some differences, they have remarkably similar appearances to those of the entire spaces of geometric or equilateral knots as reported elsewhere (see e.g. [25, 11, 15, 6, 17]).

The large scale similarity between the appearance of the local data, that is the knot populations nearby the thick unknot, trefoil knot, and figure-eight knot, and the equilateral and geometric knot populations suggests that these populations may be related via a “change of scale,”

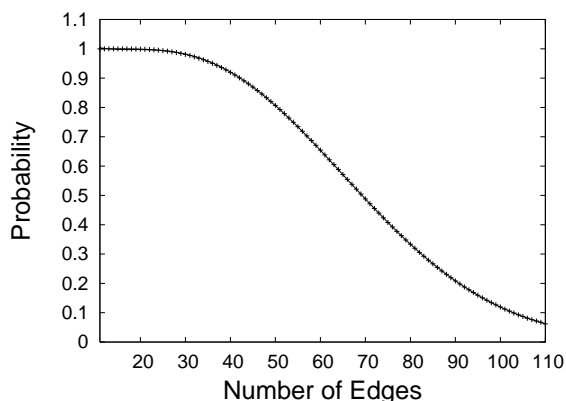


FIGURE 9. Probability of trivial knots versus the number of edges in the unknot tube.

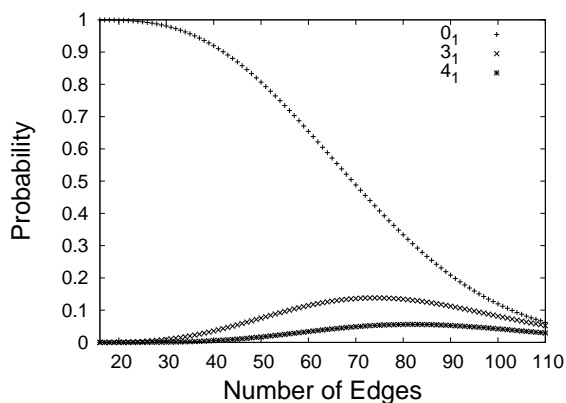


FIGURE 10. Probability of knotting versus the number of edges in the unknot tube.

perhaps a homeothety given by a translation and an expansion or contraction taking  $n$  to  $a + bn$ , where  $b$  determines the change of scale. One test of this hypothesis is to use the monotonically decreasing data for the unknot to create a functional correspondence between the number of edges for the perturbations of the unknot and those of the thick trefoil. We did this by fitting a cubic spline to the unknot data for perturbations within the thick trefoil knot and using a binary search to estimate the number of edges within the unknot tube needed to achieve the same probability. We then fit the correspondence with a linear function. The scale change function derived by application of this strategy to the perturbations of the trivial knot and those of the trefoil knot is shown in Figure 15. The initial behavior of the scale change function is incompatible with a universal change of scale. In

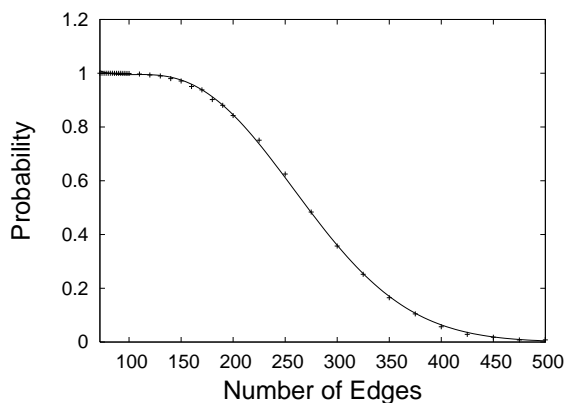


FIGURE 11. Probability of compositions with the trivial knot versus the number of edges in the trefoil tube.

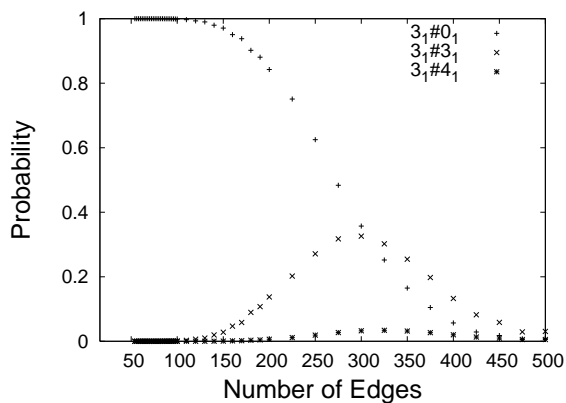


FIGURE 12. Probability of knotting versus the number of edges in the trefoil tube.

the range beyond this, larger than 20 edges, the unknot data support a change of scale. Note that for a very large number of edges, towards the asymptotic range, a change of scale would be expected since four consecutive vertices will be close to lying on a straight line segment (in which case a perturbation of 1.5 times the edge length will be sufficient for the vertices to coalesce). In the present case the potential scale change function is approximately

$$39.8444 + 3.3127n$$

with an R-squared value of 0.998. Looking closely at the data in Figure 15, one might propose a more complex structure consisting of an initial range in which the data is sparse, a second range until about 60 edges governed by finite size considerations, and a subsequent range

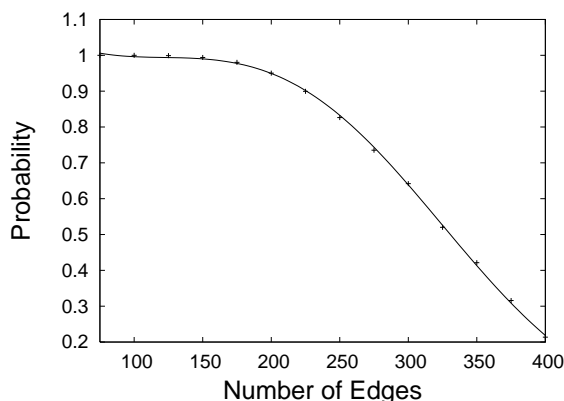


FIGURE 13. Probability of compositions with the trivial knot versus the number of edges in the figure-eight tube.

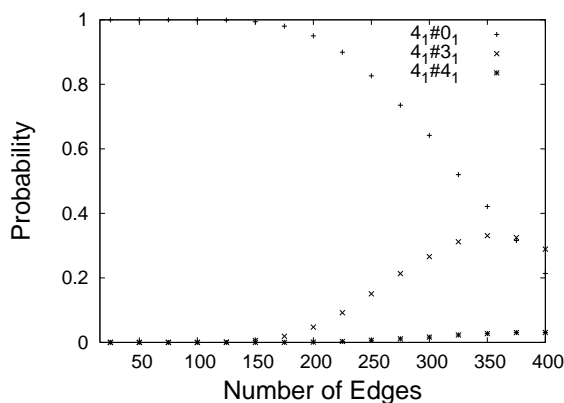


FIGURE 14. Probability of knotting versus the number of edges in the figure-eight tube.

governed by asymptotic size behavior. The transition from finite range to asymptotic range structures remains quite obscure and, we propose, worthy of deeper investigation.

A critical test of the hypothesis that a change of scale captures the differences local and global structures of knot space is the success or failure of the change to capture the properties of the non-trivial knot types. The same change of scale is applied to the trefoil knots in Figure 16 and figure-eight knots in Figure 17 for these perturbations. The maximal values of the associated knot probabilities have been rescaled to one to capture the degree to which the shapes of these knot probability functions are scale invariant. While the fit is reasonable, it does not give compelling evidence of the hypothesized scale change in as much as the trefoil perturbation probabilities are both shifted slightly

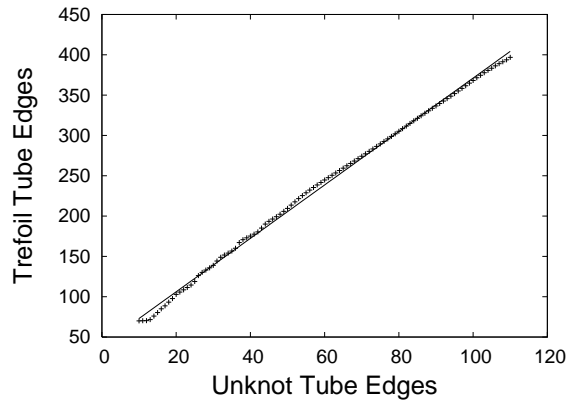


FIGURE 15. The correspondence between the number edges for perturbations within the and trefoil tubes derived by means of the proportion of compositions with the trivial knot.

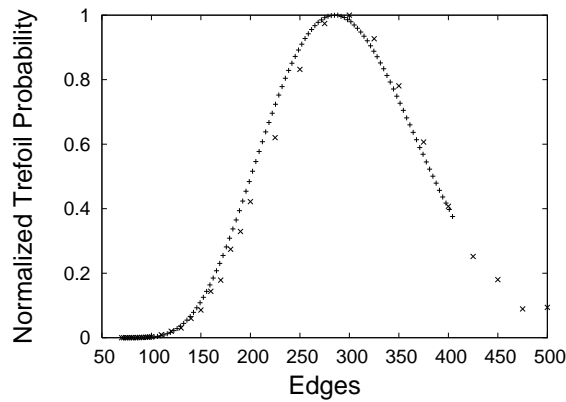


FIGURE 16. The trivial to trefoil perturbation change of scale applied to compositions of trefoils.

toward a larger number of edges. Thus, one expects that even the local knot probabilities will be influenced by the geometric properties of the core knot.

## 6. COMPLEXITY TRANSITIONS

This section concerns the increase in the complexity of observed knotting as the number of edges increases while, roughly, keeping the thickness constant. For small numbers of edges the curves are so tight that no knotting is possible, but as the number of edges increases, knotting

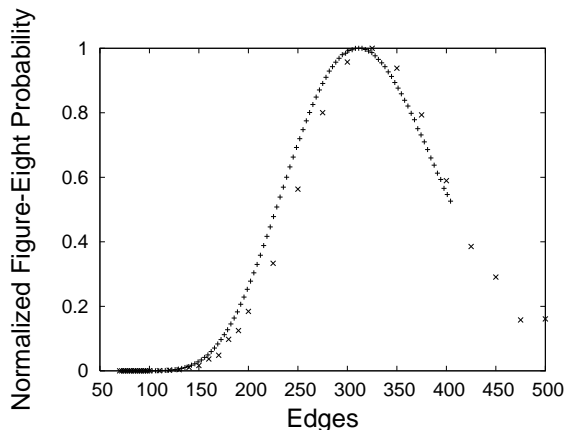


FIGURE 17. The trivial to trefoil perturbation change of scale applied to compositions of figure-eights.

becomes possible. One of the classic theorems shows that the probability of any number of trefoil summands goes to one and the number of edges tends to infinity. It is in this context that one is lead to track the number of trefoil summands that are actually observed in the data. One expects this number to increase as the number of edges increases, but at what rate? Keeping track of this, we find that the observed occurrence is quite regular. The experimental data, shown in Figure 18, suggest that, for the unknot, the number of trefoil summands is given by  $\lfloor \frac{n-4}{8} \rfloor$ , where  $\lfloor x \rfloor$  denotes the integer part of  $x$ . The fact that eight edges seems to be required for additional trefoil summands is consistent with our earlier theoretical estimates and the experimental data giving the first observation of a trefoil in the perturbations of the unknot at nine edges. The fact that only four additional edges are theoretically required to add another trefoil summand is offset by the exceedingly small probability that additional knotting will occur in a random sample. Thus, the requirement of an additional edges is probabilistic observation and not a theoretical consequence of the geometry. The extent to which these transition numbers depend upon the geometry of the core knot is an interesting question.

## 7. THE TUBE THEOREM

Let  $Tube(e_i, r)$  be the union of closed balls of radius  $r$  about each point on the edge  $e_i$  and  $Tube(K, r)$  be the union of  $Tube(e_i, r)$  over each edge  $e_i$ . We will show that  $Tube(K, r)$  is an embedded torus when  $r < R(K)$ , which insures that all of the perturbation data discussed earlier, is in fact local knotting.

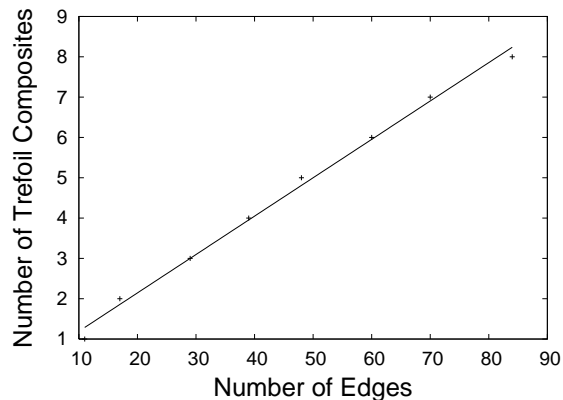


FIGURE 18. The observed number of trefoil summands as a function of the number of edges in perturbations of the unknot in samples of size  $5 \times 10^6$ .

Recall, in [14], the thickness radius of a smooth knot was defined as the largest radius of a non self-intersecting tube about the knot. The thickness radius was then characterized in terms of local disk intersections, detected by *MinRad*, and arclength-distant disk intersections, detected by half the double-critical self-distance (abbreviated *dcsd*). Polygonal thickness radius was defined [23, 22] to model *MinRad* and *dcsd* for polygons and, thus, is based on the characterization of thickness radius for smooth knots. The following theorem unites polygonal thickness radius with the origins of thickness radius in terms of tubular neighborhoods.

**Theorem 7.1.** *If  $r < R(K)$ , then  $\text{Tube}(K, r)$  is an embedded torus.*

The proof of this theorem follows later in this section. Fix an  $r < R(K)$ . We begin by analyzing the components which make up  $\text{Tube}(K, r)$ . The tube about one edge  $\text{Tube}(e_i, r)$  consists of a cylinder with two hemiballs attached at the ends and resembles a pill (see Figure 19).

We cut each pill along a particular angle bisecting plane at each of its vertices to create  $n$  cells and show that non-adjacent cells are disjoint. We construct a cell  $B_i$  along  $e_i$  as follows: At a vertex  $v_i$ , the adjacent edges  $e_{i-1}$  and  $e_i$  form a plane, say  $Q_i$ . Let  $P_i$  be the plane that bisects the angle at  $v_i$  and contains a normal to the plane  $Q_i$ . The planes  $P_i$  and  $P_{i+1}$  divide space into three (in the non-generic case where two consecutive edges are collinear) or four regions. Let  $B_i$  be the closure of  $\text{Tube}(e_i, r)$  intersected with the region which contains  $e_i$ . An example of a cell is shown in Figure 20.

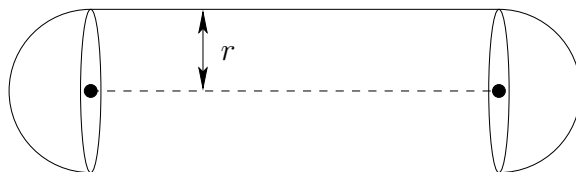


FIGURE 19. The tubular neighborhood  $Tube(e_i, r)$  of one edge (represented by the dashed line) is a cylinder with hemiball endcaps and resembles a pill.

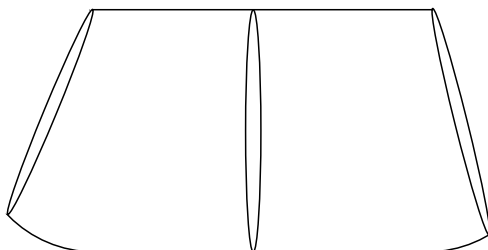


FIGURE 20. A cell is constructed by cutting  $Tube(e_i, r)$  along angle bisecting planes at its two vertices.

So what do these cells look like? We begin by dividing each cell into several pieces.

Consider two adjacent cells, say  $B_1$  and  $B_2$  corresponding to the edges  $e_1$  and  $e_2$  and vertices  $v_1, v_2$ , and  $v_3$  (see Figure 21). Suppose  $x$  is on the boundary of  $B_1$ . Then the minimum distance between  $x$  and  $e_1$  must be  $r$  or  $x$  is on one of the planes that bounds  $B_1$ , that is  $P_1$  or  $P_2$ . Suppose the former. Then the point  $y \in e_1$  minimizing the distance between  $x$  and  $e_1$  is either a non-vertex or a vertex point. If  $y$  is a non-vertex point, then  $x$  lies on the boundary circle of the normal disk to  $e_1$  centered at  $y$  of radius  $r$ , i.e. on the cylinder boundary portion of  $B_1$ . If  $y$  is a vertex point, then  $x$  lies on the hemisphere of radius  $r$  centered at  $y$ , the sphere boundary portion of  $B_1$ .

We will look at the  $B_1$  boundary points lying on  $P_1$  and  $P_2$  later. For now, we analyze the cylinder and sphere portions of the boundary of  $B_1$ .

At the vertex  $v_2$ , we will show that the sphere boundary points form a spherical wedge. Let  $H_1$  be the endcap hemiball of radius  $r$  at  $v_2$  from  $Tube(e_1, r)$  and  $H_2$  be the endcap hemiball of radius  $r$  at  $v_2$  from  $Tube(e_2, r)$ . If  $x$  is a vertex boundary point, then  $x$  must be an element of  $H_1$  and  $H_2$ . This set  $H_1 \cap H_2$  is bounded by the two disks centered at  $v_2$  that are normal to  $e_1$  and  $e_2$  respectively (see Figure 22). The



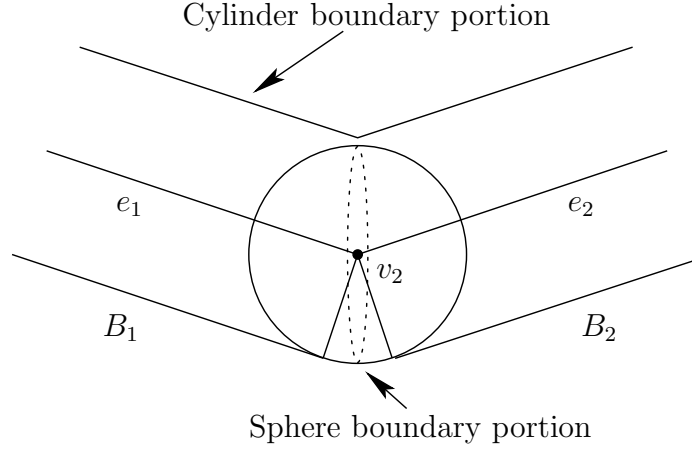


FIGURE 21. The corner section where two cells meet.

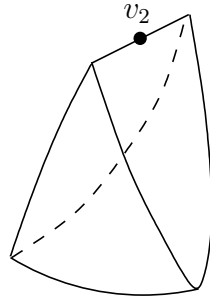


FIGURE 22. One full spherical wedge.

intersection  $H_1 \cap H_2$  forms a spherical wedge of interior angle  $\pi - \text{angle}(v_2)$ . The plane  $P_2$  splits this wedge into two isometric pieces, one belonging to  $B_1$  and one belonging to  $B_2$ . The boundary of the wedge (and the two half-wedges cut by  $P_2$ ) consists of points on the hemisphere and two semidisks. Note that one of these semidisks is connected to the cylinder of  $B_1$  and the other is connected to the other half of the spherical wedge belonging to  $B_2$ .

The following lemma will play a crucial role in the proof of the Tube Theorem. Let  $P_i^-$  and  $P_i^+$  be the planes centered at  $v_i$  normal to  $e_{i-1}$  and  $e_i$  respectively (see Figure 23). Note that  $P_i^-$  splits  $\mathbb{R}^3$  into two closed half-spaces, each containing  $P_i^-$ . Let  $\text{Half}_i^-$  be the half-space containing all of  $e_i$ . Define  $\text{Half}_i^+$  similarly so that  $e_i$  is contained in  $\text{Half}_i^+$ .

**Lemma 7.2.** *If  $x \in \text{Half}_i^- \cap \text{Half}_i^+$ , then the minimum distance from  $x$  to both  $e_{i-1}$  and  $e_i$  is realized at  $v_i$ . In particular, if  $x \in H_{i-1} \cap H_i$ ,*

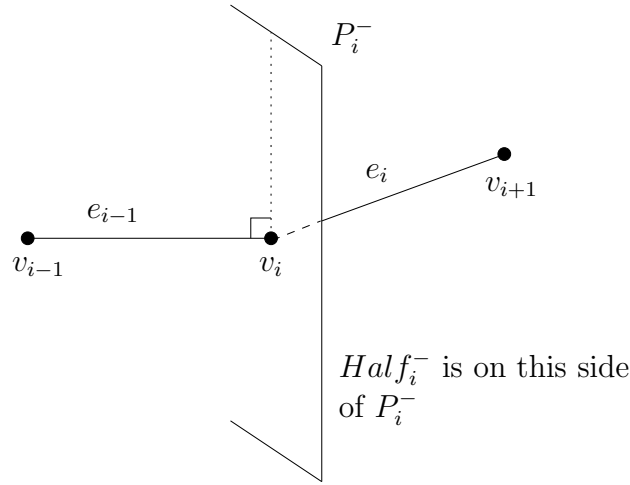


FIGURE 23. The plane  $P_i^-$  is normal to  $e_{i-1}$  at  $v_i$ .

then the minimum distance from  $x$  to both  $e_{i-1}$  and  $e_i$  is realized at  $v_i$ .

*Proof.* It is clear that if  $x \in \text{Half}_i^-$ , the distance from  $x$  to  $e_{i-1}$  is minimized at  $v_i$ . Similarly, if  $x \in \text{Half}_i^+$ , the distance from  $x$  to  $e_i$  is minimized at  $v_i$ . Thus, if  $x \in \text{Half}_i^- \cap \text{Half}_i^+$ , then the distance from  $x$  to both  $e_{i-1}$  and  $e_i$  is minimized at  $v_i$ . The second part of the theorem follows immediately.  $\square$

While the sphere boundary's two semidisk faces (just the portion of the wedge lying in  $B_1$ ) connect smoothly to the cylinder and other spherical wedge, some of the cylinder boundary points connect in a more transverse fashion. The set of cylindrical boundary points for  $B_1$  consists of the points on the cylinder along  $e_1$  minus the portions cut off by the planes  $P_1$  and  $P_2$ . We concentrate on the end with  $P_2$  passing through  $v_2$ . Since  $r < R(K) \leq \text{MinRad}(K)$  and by the definition of  $\text{MinRad}(K)$ , the plane  $P_2$  can only intersect the cylinder about  $e_1$  on the normal disks of the cylinder associated to the points between the midpoint of  $e_1$  and  $v_2$ . In other words,  $P_1$  and  $P_2$  do not intersect within  $\text{Tube}(e_1, r)$ . This observation allows us to analyze this portion of  $B_1$  further. The plane  $P_2$  passes through  $v_2$  and bisects the angle at  $v_2$ . Thus, the intersection of  $P_2$  and the cylinder forms a half-ellipse whose minor axis has length  $2r$  and major axis has length  $2r \sec \frac{\text{angle}(v_2)}{2}$ , which is at least  $2r$ . The minor axis is the intersection of the disk centered at  $v_2$  normal to  $e_1$  with the plane determined by  $e_1$  and  $e_2$ , and coincides with the bounding diameter of the semidisk of the

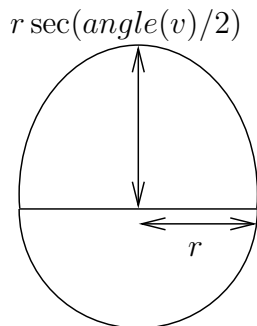


FIGURE 24. Cutting a cell along the bisecting plane at a vertex yields a semicircle connected to an ellipse along the diameter of the circle.

wedge. Thus, at this end of  $B_1$ , the boundary of the cylindrical portion is a semidisk with a half-ellipse intersecting at an angle of  $\frac{\pi - \text{angle}(v_2)}{2}$  (see Figure 24).

The entire cell  $B_1$  consists of a cylinder cut by two planes (revealing two half-ellipses) with two spherical wedges added. We will show that non-consecutive cells are disjoint. We do this by splitting the boundary of the cell into the following components:

- the two half-ellipses of the cut cylinder (cylinder faces)
- the remaining cylinder points of the cylinder boundary of the cell (cylinder surface)
- the two semidisk boundaries of the sphere wedge (wedge face)
- the round spherical portion of the sphere wedge (wedge surface)

Note that the points on the cylinder surface form an open two-manifold. The points on the wedge surface also form an open two-manifold. By the discussion above, adjacent cells intersect only along the plane bisecting their mutual vertex angle. This intersection is the union of a half-ellipse and semidisk (from Figure 24) joined along the minor axis and diameter respectively.

By the definition of  $\text{MinRad}(K)$ , normal disks of adjacent edges centered at their respective midpoints intersect at a radius  $r \geq \text{MinRad}(K) \geq R(K)$ . Since  $r < R(K) \leq \text{MinRad}(K)$ , the normal disks of radius  $r$  centered at the midpoints of  $e_i$  and  $e_{i+1}$  do not intersect. Thus, the cell  $B_i$  is connected and convex. We will paste these cells together to form  $\text{Tube}(K, r)$ . We are now ready to prove Theorem 7.1.

**Theorem 7.1.** *If  $r < R(K)$ , then  $\text{Tube}(K, r)$  is an embedded torus.*

*Proof.* Clearly,  $\text{Tube}(K, r) = \cup_i B_i$ . We will show that non-consecutive cells are disjoint. Let  $r$  be the minimal radius such that the intersection of a pair of non-consecutive cells is non-empty. We show that either  $r \geq R(K)$  or  $r$  is not minimal, to obtain a contradiction. Suppose  $B_i$  and  $B_j$  ( $i, j$  non-consecutive) intersect. Since  $r$  is minimal, this intersection must occur on the boundary of  $B_i$  and  $B_j$ . Let  $x \in B_i \cap B_j$ .

The remainder of this proof is split into several cases, each one covering a situation where  $x$  is in a different part of the boundary of  $B_i$  and  $B_j$ . First, we cover the intersections between surfaces. Note that all of these points lie on the boundary of the cylinder or spherical wedge and are distance exactly  $r$  from  $K$ .

**Case:** Cylinder surface to cylinder surface

If the tangent planes of the cylinders at  $x$  are not identical, then one of the cylinders pierces the other cylinder, that is, the interiors of the three-dimensional filled cylinders intersect. Thus, there is an intersection between the cylinders at a radius smaller than  $r$ . This contradicts that assumption that  $r$  is minimal.

If the tangent planes coincide, then there exists  $x_i \in e_i$  and  $x_j \in e_j$  such that  $x, x_i$ , and  $x_j$  are collinear and  $e_i \perp \overline{x_i x_j} \perp e_j$ . Thus,  $(x_i, x_j)$  is a doubly critical pair. This implies  $\|x_i - x_j\| \geq 2R(K)$  and  $r \geq R(K)$ .

**Case:** Cylinder surface to wedge surface

As above, if the tangent planes do not coincide, then the cylinder pierces the wedge. This contradicts the fact that  $r$  is minimal.

So suppose the tangent planes coincide. Without loss of generality, we can assume that the wedge is a part of  $B_i$  and the cylinder is a part of  $B_j$ . Then there exists a vertex  $v \in e_i$  (whichever of  $v_i$  or  $v_{i+1}$  determine the spherical wedge) and a point  $x_j \in e_j$  such that  $\overline{v x_j} \perp e_j$ . By Lemma 7.2, the pair  $(v, x_j)$  is actually doubly critical. This implies  $\|v - x_j\| \geq 2R(K)$  and  $r \geq R(K)$ .

**Case:** Wedge surface to wedge surface

If the tangent planes do not coincide, then the wedges intersect at a smaller radius and  $r$  is not minimal.

Suppose the tangent planes coincide. Let  $u$  and  $v$  be the vertices corresponding to the wedges. By Lemma 7.2 (applied twice),  $(u, v)$  forms a doubly critical pair and we have  $r \geq R(K)$ .

**Case:** Wedge face to wedge surface and cylinder surface

The semidisk face of the half-wedge intersects smoothly with the adjacent edge's half-wedge. Thus, any intersection on this semicircle boundary is the same as a wedge surface intersection. Any intersection of the remaining portion of the disk must intersect the interior of one of the two adjacent half-wedges. This would contradict that  $r$  is minimal.

**Discussion of the cases:** Cylinder face to anything

The intersection of the half-ellipse and the semidisk, a line segment which is the minor axis and bounding diameter respectively, can be considered as a part of the semidisk and are covered by the argument above. We restrict our attention to the remaining half-ellipse points.

We will show that nothing can intersect the points on the half-ellipse without contradicting the assumption that  $r$  is minimal. The cylinder face corresponds to two adjacent cut cylinders, say  $B_i$  and  $B_{i+1}$ , so we will consider the region formed by the union of their cut cylinders (which is bounded, in part, by the boundary of the common half-ellipse). If the turning angle at the vertex is 0, then the adjacent edges are collinear and the union of the two cells is cylindrical in a neighborhood of the half-ellipse (which would be a semicircle in this case). So suppose this angle is not 0. Then the tangent planes at any half-ellipse boundary point do not coincide. If  $x$  is a half-ellipse point, then any disk centered at  $x$  lies partially within either  $B_i$  or  $B_{i+1}$  (or both). In other words, there is a crease between the adjacent cells. We continue with the four remaining cases.

**Case:** Cylinder face to cylinder or wedge surface

Let  $D$  be a small disk centered at  $x$  lying on the tangent plane of the cylinder or wedge surface at  $x$ . Then  $D$  intersects the interior of  $B_i$  or  $B_{i+1}$  at a radius smaller than  $r$ , which is a contradiction.

**Case:** Cylinder face to wedge face

Again, the faces of the wedge can attach smoothly to the cylinder and wedge surface. Thus, this case is covered by the previous argument.

**Case:** Cylinder face to cylinder face

Let  $D$  be a disk centered at  $x$  lying entirely within  $B_i$  (there are many of these). By the observation above, this disk must intersect the interior of  $B_j$ . Thus, the interior of  $B_i$  intersects the interior of  $B_j$ , which implies that  $r$  is not minimal.  $\square$

The previous result is sharp in the sense that for any polygonal knot in which  $R(K) = dcsd(K)/2 \leq MinRad(K)$ , any slightly larger neighborhood will necessarily no longer be an embedded torus. While this result has not been shown for polygons, Durumeric [8] has shown that ropelength-minimized smooth knots necessarily have  $dcsd(K)/2 \leq MinRad(K)$ . Furthermore, our construction yields a canonical strong deformation retract from the tube to the knot. This can be obtained by “fanning” over the points in the cut portion of the cells and sending the remainder of the points (i.e. points which lie on a normal disk where all of the normal disk lies inside a particular cell) to the center of the disk.

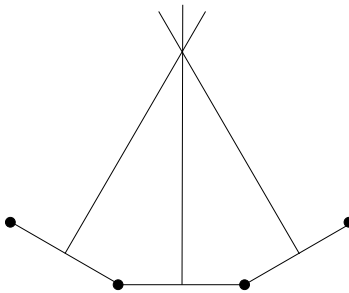


FIGURE 25. When  $r$  is larger than  $MinRad(K)$ , the tube extends beyond the intersection of the perpendicular bisectors of the edges.

However, if the thickness radius is controlled strictly by the  $MinRad$  term, a radius  $r$  slightly larger than  $R(K)$  can still be an embedded torus. If  $r > MinRad(K)$ , then a pair of consecutive planes, say  $P_i$  and  $P_{i+1}$ , will meet in the interior of  $Tube(K, r)$  (see Figure 25). While  $Tube(K, r)$  could still be an embedded torus, we lose the canonical strong deformation retract from this torus to the knot. The smooth thickness radius has this same behavior.

Furthermore, it is possible that for some  $r > R(K)$ , the tube  $Tube(K, r)$  is an embedded torus. Imagine a small, tight trefoil in what would otherwise be a large circle. When  $r$  is sufficiently large to “fill-in” the volume around the trefoil, there is an interval of radii for which the solid will be an embedded torus. The radii at which such phase changes occur may be of independent interest. In particular, these critical radii determine scales at which different satellite structures of local knotting can appear.

## 8. CONCLUSIONS

The theoretical and computational explorations of knots near thick equilateral trivial, trefoil, and figure-eight knots in the space of geometric knots provide a clear picture of the growth of complexity. While small perturbations give topologically equivalent knots, with increasing size of perturbation the complexity of knotting encountered grows rapidly all the while remaining within the tubular neighborhood of the knot. We have shown, in Theorem 7.1, that this neighborhood can be understood as the union of balls centered at points of the core knot and have established relationships between the length of the edges and the thickness radius of the knot that gives structure to the increase of complexity with increasing size of perturbation. These knots are all satellites of the core knot and are most likely, as is demonstrated by

our simulation data, to be connected sums of the core with local knots in the tube.

A numerical study of the growth of knotting about the thick knots shows significant qualitative similarity that might be an indication of a change of scale between the neighborhoods. Testing this hypothesis with the cases of the trivial and trefoil tube perturbations, we see evidence of this possibility but, also, a distinct shift in structure that indicates that this may not be true due to the finite range behavior of the knotting distributions.

The numerical study confirms and quantifies the structure of local summands by testing the growth of trefoil summands in the perturbations of the trivial knot. With each additional eight edges one is likely to see the possibility of an additional trefoil sum in a sample of size  $5 \times 10^6$ .

There are several interesting questions that are suggested by the results of this project. First, the extent to which the geometry of the core knot influences the complexity of the knotting arising from small perturbations is suggested in our work but, we believe, there may be stronger connections to be uncovered even in the case where the knot structure is relatively homogeneous. Secondly, our work on perturbations describes knotting near a thick knot in the space of geometric knots but does not have any direct implications on the neighborhood of the knot in the space of equilateral knots. Such a study would be interesting and important as we would expect the limitation to equilateral knots to promote a much more rigid structure than that reflected in the free perturbations. Third, as we have discussed elsewhere [18], the knot data in this study lies within the “finite range,” arguably before the domination of the exponential decay that defines the asymptotic range of knotting. Already, in this finite range, one finds great complexity in the knotting structure. Explorations that give high quality data in the asymptotic range may, one imagines, give a qualitatively different picture. Fourth, in this work we have investigated the structure of “local knotting,” the summands which occur within the tube surrounding the core knot. We have not yet observed non-summand satellites that are theoretically possible but unlikely. What happens, we wonder, if one moves into the global knotting regime by allowing perturbations that extend beyond the frontier of the tube.

#### ACKNOWLEDGMENTS

Piatek and Rawdon were supported by NSF Grant #DMS0311010.

## REFERENCES

- [1] Gregory Buck and Jeremy Orloff. A simple energy function for knots. *Topology Appl.*, 61(3):205–214, 1995.
- [2] J. A. Calvo. *Geometric knot theory: the classification of spatial polygons with a small number of edges*. PhD thesis, University of California, Santa Barbara, 1998.
- [3] Jorge Alberto Calvo. Geometric knot spaces and polygonal isotopy. *J. Knot Theory Ramifications*, 10(2):245–267, 2001. Knots in Hellas '98, Vol. 2 (Delphi).
- [4] Jason Cantarella, Robert B. Kusner, and John M. Sullivan. On the minimum ropelength of knots and links. *Invent. Math.*, 150(2):257–286, 2002.
- [5] S. S. Chern. Curves and surfaces in Euclidean space. In *Studies in Global Geometry and Analysis*, pages 16–56. Math. Assoc. Amer. (distributed by Prentice-Hall, Englewood Cliffs, N.J.), 1967.
- [6] Tetsuo Deguchi and Kyoichi Tsurusaki. Topology of closed random polygons. *J. Phys. Soc. Japan*, 62(5):1411–1414, 1993.
- [7] O. Durumeric, R. A. Litherland, E. Rawdon, and J. Simon. Thickness of knots 2. preprint.
- [8] Oguz C. Durumeric. Local structure of ideal shapes of knots. arXiv:math.GT/0204063, 2002.
- [9] Bruce Ewing and Kenneth C. Millett. Computational algorithms and the complexity of link polynomials. In *Progress in knot theory and related topics*, pages 51–68. Hermann, Paris, 1997.
- [10] Herbert Federer. Curvature measures. *Trans. Amer. Math. Soc.*, 93:418–491, 1959.
- [11] M. D. Frank-Kamenetskiĭ and A. V. Vologodskiĭ. Topological aspects of the physics of polymers: the theory and its biophysical applications. *Sov. Phys. Usp.*, 24:679–695, 1981.
- [12] Oscar Gonzalez and John H. Maddocks. Global curvature, thickness, and the ideal shapes of knots. *Proc. Natl. Acad. Sci. USA*, 96(9):4769–4773 (electronic), 1999.
- [13] Otto Krötenheerdt and Sigrid Veit. Zur Theorie massiver Knoten. *Wiss. Beitr. Martin-Luther-Univ. Halle-Wittenberg Reihe M Math.*, 7:61–74, 1976.
- [14] R. A. Litherland, J. Simon, O. Durumeric, and E. Rawdon. Thickness of knots. *Topology Appl.*, 91(3):233–244, 1999.
- [15] J. P. J. Michels and F. W. Wiegel. On the topology of a polymer ring. *Proc. Roy. Soc. London Ser. A*, 403(1825):269–284, 1986.
- [16] K. C. Millett. Monte carlo explorations of polygonal knot spaces. In C. McA. Gordon, V. F. R. Jones, L. H. Kauffman, S. Lambropoulou, and J. H. Przytycki, editors, *Proceedings of the International Conference on Knot Theory and its Ramifications held in Delphi, August 7–15, 1998*, Singapore, 2001. World Scientific Publishing Co.
- [17] Kenneth C. Millett. Knotting of regular polygons in 3-space. *J. Knot Theory Ramifications*, 3(3):263–278, 1994. Random knotting and linking (Vancouver, BC, 1993).
- [18] Kenneth C. Millett and Eric J. Rawdon. Universal characteristics of polygonal knot probabilities. In Jorge A. Calvo, Kenneth C. Millett, Eric J. Rawdon, and



- Andrzej Stasiak, editors, *Physical and Numerical Models in Knot Theory*, Ser. Knots Everything, pages 247–274. World Sci. Publishing, Singapore, 2005.
- [19] Alexander Nabutovsky. Non-recursive functions, knots “with thick ropes”, and self-clenching “thick” hyperspheres. *Comm. Pure Appl. Math.*, 48(4):381–428, 1995.
- [20] Jun O’Hara. Family of energy functionals of knots. *Topology Appl.*, 48(2):147–161, 1992.
- [21] Michael Piatek and Eric J. Rawdon. TOROS. <http://www.mathcs.duq.edu/~rawdon>. Program for visualizing, manipulating, and thickness maximizing knots.
- [22] Eric J. Rawdon. Approximating the thickness of a knot. In *Ideal knots*, pages 143–150. World Sci. Publishing, River Edge, NJ, 1998.
- [23] Eric J. Rawdon. Approximating smooth thickness. *J. Knot Theory Ramifications*, 9(1):113–145, 2000.
- [24] Eric J. Rawdon. Can computers discover ideal knots? *Experiment. Math.*, 12(3):287–302, 2003.
- [25] A. V. Vologodskiĭ, A. V. Lukashin, M. D. Frank-Kamenetskiĭ, and V. V. Anshelevich. The knot problem in statistical mechanics of polymer chains. *Ž. Èksper. Teoret. Fiz.*, 66(6):2153–2163, 1974.

DEPARTMENT OF MATHEMATICS, UNIVERSITY OF CALIFORNIA, SANTA BARBARA, SANTA BARBARA, CA 93106, USA, EMAIL: MILLETT@MATH.UCSB.EDU

DEPARTMENT OF COMPUTER SCIENCE AND ENGINEERING, UNIVERSITY OF WASHINGTON, SEATTLE, WA 98195, USA, EMAIL: PIATEK@CS.WASHINGTON.EDU

DEPARTMENT OF MATHEMATICS AND COMPUTER SCIENCE, DUQUESNE UNIVERSITY, PITTSBURGH, PA 15282, USA, EMAIL: RAWDON@MATHCS.DUQ.EDU